Journal Pre-proofs

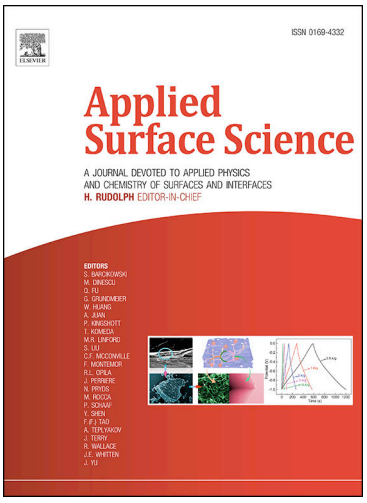

Full Length Article

Cu oxidation mechanism on Cu-Zr(O)N coatings: Role on functional properties

José D. Castro, Maria J. Lima, Isabel Carvalho, Mariana Henriques, S. Carvalho

PII: S0169-4332(21)00780-7
DOI: https://doi.org/10.1016/j.apsusc.2021.149704
Reference: APSUSC 149704

To appear in: *Applied Surface Science*

Received Date: 3 February 2021
Revised Date: 20 March 2021
Accepted Date: 27 March 2021

Please cite this article as: J.D. Castro, M.J. Lima, I. Carvalho, M. Henriques, S. Carvalho, Cu oxidation mechanism on Cu-Zr(O)N coatings: Role on functional properties, *Applied Surface Science* (2021), doi: https://doi.org/10.1016/j.apsusc.2021.149704

Cu oxidation mechanism on Cu-Zr(O)N coatings: Role on functional properties

José D. Castro[1]*, M. J. Lima[1], Isabel Carvalho[1,2,3], Mariana Henriques[3], S. Carvalho[2,1].

[1] CFUM-UP, Centro de Física das Universidades do Minho e do Porto, University of Minho, Campus of Azurém, 4800-058 Guimarães, Portugal.

[2] SEG-CEMMPRE Mechanical Engineering Department, University of Coimbra, 3030-788 Coimbra, Portugal.

[3] CEB, Center of Biological Engineering, LIBRO – Laboratório de Investigação em Biofilmes Rosário Oliveira, University of Minho, Campus of Gualtar, 4710-057 Braga, Portugal.

*Corresponding author

E-mail address: id8292@alunos.uminho.pt

Pernament address: Departamento de física – Escola de ciências, Universidade do Minho, Alameda da Universidade, 4800-058 Guimarães, Portugal.

ABSTRACT

Zirconium oxynitride (Zr(O)N) and Copper-Zirconium oxynitrides (Cu-Zr(O)N) were deposited by a DC reactive magnetron sputtering technique on stainless steel substrates. A duty cycle controller was used to obtain different oxygen contents in the developed films and a chemical activation procedure was carried out to obtain copper oxides. The samples were chemical and structurally characterized by SEM, EDS, XRD and XPS. Additional functional features were evaluated according to colour variation and inhibition halo tests. Zr(O)N and Cu-Zr(O)N surfaces showed a wide colour variation from golden to black tones, progressing through intermediate tones such as purple, blue and 'bluish' grey. An antibacterial effect was only obtained after the chemical activation of Cu-ZrON-DC100, which showed a Zr(O)N matrix incapable of catching more oxygen from deposition. After, with the additional availability of O^{2-} ions, the Cu present in the coating reacted with these ions forming CuO. The antibacterial mechanism was associated with the aforementioned characterizations and ICP-OES spectroscopy. The Cu^{2+} ions release had no influence on the antibacterial effect although the presence of CuO was decisive in obtaining an antibacterial behaviour. The acquired results demonstrated a potential multifunctionality of Cu-Zr(O)N coatings, joining an aesthetical surface with an antibacterial effect.

Keywords — Antibacterial, CuO, thin films, ZrON, sputtering.

Highlights

- Zr(O)N and Cu-Zr(O)N coating systems were deposited by Reactive Magnetron Sputtering using an oxygen programmable pulse system.
- Copper oxide crystal structures were visible after chemical activation.
- XPS results reported the nature of the copper oxides on the surface and its relationship with the Zr(O)N matrix.
- The copper incorporation made it possible to achieve colour tuneable films with an antibacterial surface.

1. Introduction

Surface treatments or decorative coatings are currently relevant in a wide range of markets such as in the automotive industry (for interior and exterior parts), markets for consumer goods (mobile phones, computers, cameras, jewellery and watchmaking), for home products (bathroom equipment, handles and cutlery) and for glasses [1–3]. In all these applications, the surfaces are intended to be moderately hard, scratch resistant and to have a wide range of colours.

Amongst other characteristics, transition metal nitrides and oxynitrides have exhibited interesting mechanical [4,5], optical [6,7], anticorrosion [8] and tribological [9] properties. Transition metal oxynitrides have been developed by several authors [10–13] since, due to their binding characteristics and their properties, they can be fine-tuned to originate nitrides and the corresponding oxide. When they are part of the same system, their industrial implementation is easy and immediate, since the final properties depend only on the chemical composition (O and N contents) and these contents depend on the processing parameters, namely, the reactive gas flows, O_2 and N_2. There are numerous examples that have been developed regarding different combinations of transition metal elements (e.g., Me - Ti, Zr, Cr…) and N, O and / or C, in order to obtain coatings with excellent mechanical properties, resistance to corrosion, with a low friction coefficient and a wide range of colours. In fact, some authors have focused on obtaining a variation of colours in metal transition oxynitrides or carboxynitrides systems. Chappé et al. [14] assessed the colour variation on TiN-based coatings with C and O addition, revealing that TiN with a low oxygen content displayed a glossy golden tone but with the incorporation of oxygen, the colour changed to dark blue. By adding carbon, the colour shifted towards black tones. In fact, in a previous study [15], the authors of this investigation reported the same colour shifting in Ti(O)N coatings and also ZrN_xO_y coatings [16]. They revealed four distinct zones in Zr(O)N system: Zone I and II, where coatings were based on ZrN and performed a wide colour pallet from pale yellow or

golden tones to dark blue; Oxynitrides (zone III) and oxides (zone IV), which presented a semi-transparent optical behaviour.

The antibacterial activity can be an additional function of decorative coatings because they are constantly submitted to physical human contact. In fact, these surfaces can be vehicles for bacterial adhesion and propagation [17] (e.g., surfaces exposed to seawater, hand contact on door handles, cell phone casings, earrings, rings, watches, faucets, decorative objects, etc.). Bacterial adhesion can also cause biofilm formations on the material surface [1]. These are communities of microorganisms that strongly adhere to the surface and are very complex and hard to remove. The biofilm formation also promotes corrosion of metal surfaces, which in turn leads to their degradation [20].

Antibacterial surfaces could be applied on surgical instruments, cutlery, doorknobs, faucets, earrings, ornaments, and reusable bottle caps, amongst other products. Currently, some researchers have been studying the biocidal characteristics of transition metal nitrides or oxynitrides matrices with antibacterial agents (e.g., silver (Ag), copper (Cu) and zinc oxide (ZnO)). Chang et al. [2] incorporated Ag in a ZrON matrix through a reactive magnetron sputtering technique, which achieved an antibacterial coating with ~12 at.% Ag that was effective against Staphylococcus aureus and Actinobacillus actinomycetemcomitans, commonly found in implant-associated infections. Osés et al. [3] performed Ag and Cu doped chromium nitride (CrN) and TiN films over ceramic tiles and all films presented around 20 at.% of dopant agent on its surface, adding an antibacterial effect against S. aureus and Escherichia coli as well as noteworthy mechanical properties. Kelly et al. [18] compared tribological and antibacterial properties of CrN/Ag, ZrN/Ag, TiN/Ag and TiN/Cu nanocomposite coatings obtained by a dual pulsed magnetron sputtering equipment. Their findings showed a degradation of the tribological properties with the incorporation of softer/active materials in the nitride film. Besides that, Kelly et al. [18] showed a hostile activity to Pseudomonas aeruginosa in the zone of inhibition (ZoI) tests. Nitro-blue tetrazolium (NBT) redox dye was also used to check the antibacterial effect after the incubation process and showed a growth inhibition of S. aureus on these coatings. Baghriche et al. [19] implemented a Cu layer over TiO_2 thin film, obtaining an antibacterial effect against Escherichia coli in simulated solar exposition. According to the reported, Cu ions (specially Cu^{2+} ion) showed a strong relation with the inactivation of bacteria.

Coatings possessing Cu as an antibacterial element are an important scientific advance as they are cheaper when compared with Ag and Zn-based coatings. Another important aspect is that, according to the periodic table of sustainability recently published by the European Chemical

Society (EuChemS) [20], Ag and Zn face a serious threat in the next 100 years, contrary to what is expected from the Cu element. Amongst possible copper-based compounds, CuO has been established as an antibacterial/antifungal agent [17,21,22].

These previous studies have revealed the potential to apply transition metal nitrides or oxynitrides, commonly used in anticorrosion or mechanical applications, to extend their functionalities such as antibacterial properties. However, there is still a lack of research on the development of aesthetic coatings and antibacterial properties.

The present study sees to explore the addition of Cu to Zr(O)N films to combine aesthetical and antibacterial properties. One of the aims is to understand the effect of oxygen and copper content on the colour of the samples. Further, performing a chemical activation of Cu-Zr(O)N films to obtain Cu-antibacterial species is also a goal of the current study. This investigation is, to the best of our knowledge, the first study of Cu-Zr(O)N films which combines both decorative and antibacterial properties. The achievements of a personalized decorative layer with antibacterial activity will impulse the position of brand-new products with high industrial interest.

2. Experimental

2.1 Deposition conditions of Cu-Zr(O)N coatings

Cu-Zr(O)N coatings were deposited by DC reactive magnetron sputtering with Zr and Cu targets (200 x 100 mm^2, with a 99,9% purity). All films were sputtered on stainless steel 316L and silicon wafers. All substrates were previously sequentially cleaned with distilled water, acetone and ethanol in an ultrasonic bath for 10 minutes each in order to remove any impurity or contamination. Before the deposition, an etching process was performed on the substrates with an argon plasma (80 sccm) for 15 minutes, by applying 0.3 A to the substrate holder with a DC pulsed power source, which was set at 1536 ns on reverse time and 200 kHz of frequency applied to the substrate holder. In the sputtering process, the reactive atmosphere and some parameters were varied to produce Zr(O)N and Cu-Zr(O)N films according to table 1. Prior to any deposition, a first Zr interlayer was deposited in an Ar atmosphere (0.64 Pa) for 15 minutes with 50 A/m^2 as the current density to promote film adhesion. An additional ZrN interlayer, was deposited for 5 minutes before the Zr(O)N and Cu-Zr(O)N coatings in order to reduce superficial defects which could produce stresses in the film and hence, possible delamination processes. A pulsed negative DC bias voltage of 50 V was applied to the substrate holder and the deposition process was carried out at 170 ºC with a base pressure of 3.3 x 10^{-4} Pa.

For the films deposition the current density applied in Zr target was 125 A/m^2 and for the films with

a copper addition a DC pulse power source (200 kHz, 1536 ns, 10 A/m^2) was used. To control the O/N ratio and consequently tune the colour pallet, a duty cycle controller was used with 45 s period in a square wave for O_2 addition on the reactive atmosphere. The duty cycle used in this study was the same as that used in previous studies by the authors [15] and which has been explained in previous these studies [23–27]. The O_2 duty cycle set-ups were 20, 40, 80 (exclusively for Zr(O)N system) and 100% (only in Cu added films), which correspond to the flow values and times shown in table 1. The ZrON-DC100 sample was discarded because of a displayed interference phenomena in its appearance.

In order to promote the formation of CuO antibacterial species, which is theoretically formed in a 1:1 O/Cu ratio, an activation procedure was performed as reported by [28]. According to the Cu-O phase diagram [29], copper has a high chemical affinity with oxygen. In fact, even with a small oxygen amount at low temperatures (< 0.004 at. % O), copper enters into a structural transition zone with pure Cu and Cu_2O. Based on the information provided by the phase diagram, where CuO species could be formed to amounts higher than 33 at.% O, Cu-Zr(O)N samples were immersed in a commercial solution of sodium hypochlorite (NaClO) at 5% (w / v) for 5 minutes. Then, the samples were washed in deionized water three times in a row in order to remove the remaining oxidizing solution and air-dried (inside a flow chamber). The same procedure was carried out for the Zr(O)N samples to allow for the same conditions to be kept for the antibacterial test.

2.2 Characterization techniques

Chemical composition was established by scanning an electron microscope (SEM) in an FEI Nova 200 scanning electron microscope equipped with an EDAX Pegasus X4M detector for energy-dispersive X-ray spectroscopy (EDS). All chemical composition measurements were taken at 15 kV and were obtained from an average of three measurements.

Coating's thicknesses were carried out by 3D Optical Profilometry in a FLMETRICS Profilm 3D profilometer. The thickness measurements were performed in a 114.5 x 85.5 μm^2 sample area and the reported value is the average of 10 measurements.

Glancing Incidence X-Ray Diffraction (GIXRD) was used to report coating's structure. Bruker D8 Discover was set up in □ = 4º, with a CuKα (λ = 1.5406 nm) radiation operated at 40 kV and 40 mA with 0.04º step size. All measurements were fitted according to the Pseudo-Voigt function.

Additional chemical characterization was carried out through X-Ray photoelectron spectroscopy (XPS) using a Kratos AXIS Ultra HSA, with VISION software for data acquisition and CASAXPS software for data analysis. The analysis was carried out with a monochromatic Al Kα X-ray source (1486.7 eV), operating at 15kV (150 W), in FAT mode (Fixed Analyzer Transmission), with a pass

energy of 80 eV for survey and 40 eV for elemental spectrum. The effect of the electric charge was corrected by the reference of the carbon peak (285 eV).

The colour coordinates were evaluated with a commercial MINOLTA CM-2600d portable spectrophotometer under the standard CIE illumining D65 in steel samples. The results were represented in the CIE L*a*b* colour space and displayed in the 1976 CIE L*a*b* colour space.

The antibacterial activity of the films was tested using *Staphylococcus epidermidis* ATCC 12228 (obtained from American Type Cell Collection). Zone of inhibition (ZoI) or halo tests adapted from Kirby-Bauer method [30], were performed to evaluate the antibacterial activity of samples according to our previous study [15]. All experiments were repeated in triplicate and at least in three independent assays. After the halo test, the samples were removed and dehydrated according to the methodology mentioned in Manninen et al. [31]. Afterward, the samples were mounted in aluminium pin stubs with an electrically conductive carbon adhesive tape (PELCO Tabs). The samples were sputter-coated with gold and observed at 10 kV by scanning electron microscope (SEM) in a FEI Nova 200 scanning electron microscope.

In order to estimate the release of copper from the coatings with time, 316L SS substrates coated with Cu-Zr(O)N were immersed in 50 ml of an NaCl (3.5%) solution at room temperature, simulating a seawater exposure. A volume of 2 ml of the solution was taken after 2 and 24 hours and analysed by inductively coupled plasma optical emission spectrometry (ICP-OES – ICP PerkinElmer spectrometer model Optima 8000).

3. Results and discussion

3.1. Chemical characterization

Chemical composition, thickness and deposition rates of the coating systems are shown in table 2. The results show that, as expected, when increasing the duty cycle (DC) on the O_2 flux, it is possible to increase the oxygen content and therefore decrease the nitrogen content for both sets of samples (example, compare ZrN-DC20 with ZrN-DC80). Figure 1 shows the oxygen incorporation into the films, which is more significant in Cu-Zr(O)N films. This increase has a small impact on the deposition rate for the Zr(O)N system. It is important to highlight that, as was expected for the Cu-Zr(O)N system, the deposition rate is significantly higher than for the Zr(O)N system, since a second target of copper was used. However, the increase by almost double the deposition rate, must not only be justified by the second target as the density current is not the doubled amount (125 A/m^2 for the Zr target and only 10 A/m^2 pulsed for the Cu target). The deposition rate is clearly increased

with the addition of copper to the Zr(O)N coatings, because Cu shows higher sputtering yields comparing with Zr (2.3 and 0.7, when bombarded with Ar at 0.6 keV, respectively [32]).

Additionally, according to the elemental mapping in the Cu-ZrON-DC100 sample, the copper is distributed uniformly along the film surface and it does not form any agglomerates or nanoparticles as is shown in figure 2.

3.2. Structural characterisation

The evolution of the crystallographic structure with the increase of the oxygen content for the Zr(O)N samples was evaluated by XRD (Figure 3a). The identified crystalline phases are fcc-ZrN (face-centred cubic ICDD card no. 00-035-0753) and orthorhombic-Zr_3N_4 (ICDD card nº 00-051-0646), which are consistent with other published studies for similar coatings [10,33]. The Zr(O)N films (with low oxygen content) displayed a characteristic rock-salt structure typical of ZrN with its common peaks in (111) (the preferential orientation), (200), (220) and (311) planes. By incorporating oxygen through duty cycle increase, the Zr(O)N films lose crystallinity, which is expressed by the decrease in the peak's intensity as well as by its broadening. Indeed, this is reflected in the decreasing of grain size as shown in figure 4. The ZrN sample displayed 9 nm crystallite sizes in the preferential growth plane (111) and after, the shrinking of this crystallite was evident as the duty cycle was increased. Another point worth highlighting is that through the increase in the oxygen content there is an increase of the Zr_3N_4 phase, which becomes the dominant one in the ZrN-DC40 and ZrN–DC80 samples (11 at% and 19 at% of oxygen content). Some authors suggest that this phase results from cell expansion by incorporation of nitrogen (and oxygen) atoms in interstitial positions [34] or as a relaxed NaCl structure with some Zr vacancies. In fact, Zr(O)N the transition from ZrN phase to Zr_3N_4 occurs due to a quasi-direct exchange between the metallic/non-metallic species ratio into the film (see table 2, the Zr/(N+O) ratio).

The evolution of the crystallographic structure with the increase of the oxygen content for the Zr(O)N samples with copper incorporated was evaluated by XRD (Figure 3b). The identified crystalline phases are fcc-ZrN (face-centred cubic ICDD card no. 00-035-0753) and orthorhombic-Zr_3N_4 (ICDD card nº 00-051-0646), which are consistent with samples without copper. However, in the samples with higher oxygen contents (Cu-ZrON-DC100) a new ZrO_2 crystalline phase can be assigned with an fcc-structure coherent with ICDD no. 00-049-1642. As has already been discussed, the Cu incorporation promotes a decrease in the Zr content, implying a decrease in the metallic/non-metallic species ratio, compared to the Zr(O)N system, as a faster transition between the ZrN phase and Zr_3N_4 is expected (even this phase is possible to detected for the Cu-ZrN coating where the Zr/N ratio is 0.9). The phases' shift across coatings reveals that oxygen replaces nitrogen

due to zirconium preference to form oxides above nitrides as is demonstrated by their formation enthalpy ($\Delta H^{\circ}_{f\ ZrO_2} = -1042.8\ kJ/mol$ [35] and $\Delta H^{\circ}_{f\ ZrN} = -365.5\ kJ/mol$ [36]). Also, figure 4 demonstrates this significant structural change through the shrinking of the ZrN crystallite size until its disappearance, which leads to the appearance of ZrO_2 crystallite in the Cu-ZrON-DC100. Besides, the Cu-ZrON-DC40 has a nanocrystalline structure within a transition between a nitride and oxide behaviour. An inset on the broad peak between 28º and 36º reveals a sum of diffraction peaks corresponding to the ZrN (111) plane and the Zr_2ON_2 (222) and (004) planes corresponding to the ICDD pattern no. 01-089-8344 (Figure 3c).

Another remark related with the Cu-Zr(O)N samples is that there are no traces of Cu or copper oxides crystalline phases, notwithstanding the amount presented in the films (≈ 10 at%). This allows us to infer with high probability that these samples will not show significant antibacterial activity due to the inexistence of CuO antibacterial species [21,22,37]. This fact was confirmed by the absence of halo to *S. epidermidis* in the non-activated samples (see Figure SI. 1). In agreement with previous studies [28], an activation of Cu-Zr(O)N was performed with a commercial solution of sodium hypochlorite (5% v / v) (see experimental section) in order to confer antibacterial properties. Structural changes promoted by the activation (samples labelled with A) are shown in the XRD diffractograms presented in Figure 5. The activation with sodium hypochlorite is an oxidative process, and by the previous results observed for the Zr(O)N coatings with the incorporation of oxygen, the Zr_3N_4 crystalline phase is expected on the Cu-ZrN coating [33,38]. Some authors [16,33] reported that ZrO_xN_y coatings obtained by reactive magnetron sputtering displayed Zr_3N_4 phases when ZrN has some oxygen inclusion, and concluded that Zr_3N_4 is a poor oxygen doped structure in ZrON systems. The Cu-ZrN(A) did not show a Cu based crystalline structure after the chemical treatment, suggesting that all the oxygen was incorporated on the ZrN structure. This behaviour was not observed for the Cu-ZrON-DC100(A) sample. In the XRD patterns, it is possible to distinguish a monoclinic-CuO and orthorhombic-Cu_8O phases according to the ICDD patterns no. 00-045-0937 and no. 01-078-1588 respectively. The CuO or Tenorite plays an important role in the antibacterial activity, as has been reported in literature [17,21,22,39]. Additionally, the presence of Cu_8O or octacopper oxide is observed: a metastable copper suboxide, which is decomposed in Cu and Cu_2O species [40]. It could be considered as a transition copper oxide towards more stable species. The formation of these copper oxides could be triggered by the exposition of an oxygen-rich media such as NaClO, increasing the available oxygen to react with the latent copper inside the film. In their study, Guan et al. [40] concluded that the Cu_8O could be formed in atmospheric conditions but in a very slow kinetics. In addition, this copper oxide results

from the interstitially incorporation of oxygen, which suggests that in the sputtering process copper metastable phases could be formed with higher oxygen amounts. Indeed, the oxidative process promotes the formation of copper oxide phases only in the samples with high amounts of oxygen. With regard to the existent phases, ZrO_2 peaks displayed an intensity loss that could be due to a loss of crystallinity promoted by the sodium hypochlorite and the possible transition to form copper oxide species.

3.3. XPS analysis

In order to investigate the chemical bonding before and after the activation process, XPS analysis was performed on the surface of the Cu-ZrN and the Cu-ZrON-DC100 samples. Firstly, it was possible to observe that survey spectra did not display any significant changes amongst films, presenting Zr, Cu, O and N as main elements. These results were aligned with the composition determined by EDS. Also, no traces of Cl on the activated samples were found (survey and region of interest, ROI), which showed that all the by-products and remaining sodium hypochlorite had been removed.

In agreement with the chemical composition of the films, four ROIs were explored: N 1s, O 1s, Zr 3d and Cu 2p. The peak parameters of all these ROI's are summarized in table 3.

The N 1s spectrum of both non-activated samples is showed in Figure 6a and 6b. The Cu-ZrN (Figure 6a) displays four peaks at 395.76 eV, 397.28 eV, 399.68 eV and 403.17 eV, whereas the Cu-ZrON-DC100 (Figure 6b) shows only one strong peak at 395.76 eV. The common peak on these samples (~395.76 eV) corresponds to Zr(O)N and it is in agreement with Milosev et al. [41] who studied the electrochemical oxidation in ZrN films. They show that this peak is a contribution of the oxynitride present in the ZrN structure. Moreover, several authors [13,41–43] have linked the binding energy (BE) at around 397.3 eV on the Cu-ZrN to an N^{3-} chemical state, corresponding to the Zr-N bond, which was also confirmed in the Zr 3d spectra (Figure 7a). The peak at ~399.68 eV ($O\text{-}N_{400}$) could also be interpreted as an oxynitride present in the coatings with higher amount of oxygen (oxygen-rich oxynitride) [41,44]. The Cu-ZrN sample showed two peaks of oxynitrides, the peaks at ~399.68 eV and ~395.76 eV, which correspond to oxygen-rich and nitrogen-rich Zr(O)N species, respectively. Finally, according with Wiame et al. [43], the peak at ~403.17 eV (N_2) is attributed to nitrogen which is dissolved in the film.

As was expected, after activation the Cu-ZrN core levels suffered a slight variation in intensities in the presence of an oxygen rich surface (figure 6c). The activation/oxidation promotes an increase on the $N\text{-}O_{400}/N\text{-}O_{396}$ intensity ratio as well as on the N_2 peak. These tendencies suggest a breakdown of the rich-nitrogen species (Zr-N) into compounds with higher oxygen amounts

(Zr(O,N)), which is aligned with a nitrogen replacement by oxygen into the ZrN network in agreement with Signore et al. [11]. The Cu-ZrON-DC100 initially showed a peak corresponding with nitrogen-rich oxynitrides (figure 6b) but after activation, rich-oxygen oxynitride and dissolved N_2 peaks appear together with a weakening of the existent peak (figure 6d). This phenomenon may be explained based on the obtained results in XRD and EDS, together with the phase diagrams of Zr with O and N. The Zr has a preferential chemical affinity with O, facilitating the formation of oxynitrides in both Cu-ZrN and Cu-ZrON-DC100 films.

The Cu-ZrON-DC100 displayed a single peak that shows the presence of rich-nitrogen oxynitride. The XRD results showed a preferential ZrO_2 formation in the film but it did not show any nitrogen-associated structure (oxynitrides). This is coherent with the O-Zr phase diagram, where a 2-x:1 ratio is needed to form Zirconium Oxide (where x must be ≤ 0.44). Chemical analysis reported a ~1.5:1 ratio which suggests that Cu-ZrON-DC100 could be present in the transition zone between Zr and ZrO_2 [45]. Also, EDS results showed that the N/Zr ratio in Cu-ZrON-DC100 is 0.7:1, that it is not enough to form ZrN according to the N-Zr phase diagram (0.8 - 1:1 N/Zr ratio) [46]. Apparently, at the structure of the coating ZrO_2 was preferentially formed (Figure 5b). However, Zr(O)N species with the remaining Zr and available N were also formed, which was poorly oxidized by the residual oxygen. Through XRD, Mishima et al. [47] observed the transition from ZrO_2 to $Zr_7O_8N_4$ (oxygen-rich oxynitride) and finally to Zr_2ON_2 (nitrogen-rich oxynitride) when performing the nitridation reaction with NH_3. This allows us to identify the probable species involved on the reduction-oxidation mechanism of ZrN to ZrO_2. Our results may suggest the presence of Zr_2ON_2 on the Cu-ZrON-DC100 surface, which was possible to observe in the XRD analysis of the Cu-ZrON-DC40 sample (figure 3c).

The Zr 3d spectra displayed two main peaks at ~182.08 eV and ~184.48 eV, which corresponds to the common doublet reported for this material, 5/2 and 3/2 spin-orbit levels, respectively (figure 7). In comparison to other literature, the BE difference between these levels (ΔE_{spin}) is 2.43 eV, is very close to our measurements (2.40 eV). Some authors [13,43] reported the BE at 182 eV to ZrO_2, but based on the N 1s spectra (figure 6), it is more probable that this peak corresponds to zirconium oxynitrides (labelled as Zr(O,N)) in all coatings as reported by Milosev et al. [41]. Also, a small peak was detected exclusively in the Cu-ZrN films at ~180.25 eV. This peak corresponds to the ZrN bonding, and is coherent with the N 1s spectra analysis [41,43,48]. After activation, the samples did not display any significant change in intensity or shifting in binding energies.

Other important information was revealed by O 1s spectra (figure 8). It is possible to fit a main peak at ~529.92 eV with a shoulder at ~531.38 eV in all films. The main peak was associated to O^{2-}

because this BE is commonly associated with transition metal oxides and is difficult to differentiate if oxygen is bonded to Zr or Cu (this will be discussed later in the Cu 2p core level). However, this peak confirms the presence of reacting species in the oxynitride peaks observed in the N 1s and Zr 3d spectra and is related with the presence of ZrO_2 [11,41–43]. Further, the detected "shoulder" could be related to transitional hydroxides as was reported by Platzmann et al. [49]. According to these authors, the BE at ~531.7 eV corresponds to $Cu(OH)_2$ and OH^- species [49]. Biesinger [50], showed the O 1s BE's of copper oxides at environmental conditions and identified the $Cu(OH)_2$ at ~531.24 eV and Cu_2O at ~531.57 eV, which is a quite well accepted scenario closer to our films, where the detected BE is at an intermediate point of these values.

After activation, coatings displayed an additional peak at ~532.06 eV, which could be interpreted as the binding energy corresponding with an OH^- bond, as was expected in the treated samples [43,49,51]. The Cu-ZrN showed a shrinking in O^{2-} peak after activation in contrast to the activated Cu-ZrON-DC100, where the O^{2-} peak maintained its intensity.

However, if this were the scenario, somehow after the Cu oxidation procedure (activation process), this shoulder would increase in comparison to the main peak, and this was not sighted in our results (compare Figure 8a with figure 8c or compare Figure 8b and 8d). For the moment, this peak will be labelled as Me (O,OH) until new statements with the Cu 2p spectra are confirmed (Figure 9).

The Cu 2p spectra of selected samples are present in Figure 9. All the samples displayed the Cu^{2+} satellite peaks at approximately ~943 eV and their respective spin-orbit components (at Cu 2p1/2 position) with ΔE_{spin} ~19.82 eV [49,50]. Additionally, almost all coatings displayed two peaks at ~932.58 eV and ~934.39 eV except on the activated Cu-ZrON-DC100. According to Platzmann et al. [49], the Cu 2p3/2 peak at ~932.50 eV is related to a mixture of Cu and Cu_2O bonding species. This overlapping is supported by other authors [50,52]. On the other hand, the peak at 934.39 eV could be linked with the $Cu(OH)_2$ compound [53]. This compound is common in samples with Cu exposed to ambient conditions at short times [49] and confirms the hydration previously seen in O 1s spectra. The activated Cu-ZrON-DC100 showed a determinant change with the appearance of a pronounced peak at 934.00 eV (figure 9d). This binding energy is broadly linked in other literature as the CuO compound [49,50,52,54]. It is possible that other species such as $Cu(OH)_2$ and Cu_2O have some contribution to this peak according to what was displayed in the O 1s spectra (figure 8d), although it is difficult to determine their contribution clearly. The presence of this peak confirms the X-Ray diffraction results where Cu-ZrN and Cu-ZrN (A) samples displayed a breakdown of ZrN to zirconium oxynitrides (figure 5a). Additionally, the Cu-ZrON-DC100 and Cu-ZrON-DC100 (A) samples exhibited a rearrangement of oxygen to form Cu_8O and CuO (Figure 5b). As deposited

the Cu-ZrON-DC100 was saturated with oxygen. An additional exposure to a sodium hypochlorite solution enabled the O^{2-} ions to react with the Cu present in the coating.

During the activation process, O^{2-} ions promoted the weakling of rich nitrogen species in the Cu-ZrN film, which was confirmed by the rise in the intensity of the oxynitride peaks. Otherwise, the Cu-ZrON-DC100 did not show any ZrN structure on the surface and the O^{2-} ions reacted directly with other available transition metal in the film structure, in this case, with the Cu elements. Apparently, the capability to catch oxygen species from the Cu-ZrON-DC100 sample was influenced by a nitrogen-rich oxynitride present after the deposition process. After activation, this oxynitride evolved into an oxygen-rich oxynitride and appeared in the N_2 phase, which denotes stability in superficial oxidation. The incapability of the Cu-ZrON-DC100 to catch more oxygen promotes the formation of copper oxides at the CuO phase. According to the obtained results, the copper reacted as proposed by Huang et al. [55]. The proposed stages that pass-via Cu in Zr(O)N matrix in the present study are:

(1) Copper hydration metastable phase formation. According with Platzmann et al. [49], this hydration depends on the concentration of OH- ions available in reacting media. In our case, hydroxyl ions came from an NaOCl commercial solution, used for the activation process. Also, some hydroxyl groups are available from moisture in the air, which could influence the presence of this compound in coatings without any additional treatment. At this stage, the reaction would be:

$$2Cu^{+}(aq) + NaClO\ (aq) \rightarrow Cu_2O(s) + NaCl(aq)\ (1)$$

$$Cu_2O\ (s) + NaClO(aq) + 2H_2O(l) \rightarrow 2Cu(OH)_2(s) + NaCl(aq)\ (2)$$

(2) Transformation in the CuO stable phase from metastable $Cu(OH)_2$. In relation to this last stage, some authors have described that the reaction happens quickly under ambient conditions and with aqueous media [49,55,56].

$$Cu(OH)_2(s) \rightarrow CuO\ (s) + H_2O(l)\ (3)$$

3.4. Effect of oxygen and copper addition on the appearance of Zr(O)N films

Figure 10a displays the obtained colours varying the oxygen content for Cu-doped and undoped ZrN samples. Colour was assessed by spectrophotometry according to the 1976 CIEL*a*b* colour space. With regard to the Zr(O)N system, the colour varied from pale yellow in a sub-stoichiometric composition and reached a bright golden tone with a small inclusion of oxygen (ZrON-DC20). When

oxygen starts to replace nitrogen inside the film to form ZrO_2, this turns from a 'reddish' brown (ZrON-DC40) into a dark 'bluish' tone (ZrON-DC80). In fact, this colour variation was reported by several authors [10,16,57,58]. In the Cu-Zr(O)N system, the base colour started at an ochre or dark golden tone and with the increase of the oxygen content, the film colour changed from purple, to 'bluish' grey and after to black. It is important to emphasize that with a small amount of copper (always less than 11 at. %), the colour pallet suffered a significant shift in the luminosity parameter. The undoped system had L* values between ~45 and ~75, while the doped system had L* values ~25 to ~50 (Figure 10 b and c). Additionally, the faster replacement of nitrogen by oxygen inside the films in the Cu-Zr(O)N coatings promoted the formation of darker tones, which are quite interesting tones for different markets. Some authors have reported that the oxygen inclusion in oxynitrides with a transitional metal turned the base colour into 'bluish' tones with low luminosity [15,38,58]. Also, the presence of Cu in the coating structure promotes faster oxygen incorporation due the decrease on the Zr content.

3.5. Antibacterial tests

Samples were biologically tested according to aforementioned specifications. The choice of this strain - *Staphylococcus epidermidis* - is related to the applicability of the developed materials, since this microorganism colonizes the skin, which, because of exposure to hands, is in direct contact with decorative and aesthetic materials.

As expected, undoped systems did not show any effect against *S. epidermidis* (Figure 11a). In relation to the doped films, initially the halo test revealed that no sample presented antibacterial properties, since none showed an inhibition zone (clean zone around the sample without bacteria) (see figure S1). This was true even for samples with a high copper content. However, since copper is described as being widely used as an antibacterial agent [59,60] and since all samples had an important copper content in an amorphous form, we decided to perform an activation of copper with a commercial solution of sodium hypochlorite (NaClO) at 5% (w / v). In fact, this activation worked but only with the Cu-ZrON-DC100 sample, which presented a clear halo around itself after the activation process, as showed in the figure 11b. Through the SEM images obtained after the halo test, it is also possible to see the total absence of bacteria on the surface of this sample (figure 11b (i)), while the sample Cu-ZrN (A) (figure 11a (i)) shows a vast bacterial colonization.

In an attempt to better understand the role of this activation and the reason behind it only being effective in one sample, XRD, XPS and ICP were performed. As mentioned previously, XRD results showed that only the Cu-ZrON-DC100 (A) sample displayed Cu in an oxide form (figure 5b), which contributes to promote the formation of antibacterial agents with copper as CuO [21,22,39].

Moreover, XPS results confirmed the CuO presence on the Cu-ZrON-DC100 (A) sample surface (figure 9d). As expected, ICP results (figure 12) showed a higher Cu^{2+} release in the Cu-ZrN sample (740 ppb) than in the Cu-ZrON-DC100 sample (351 ppb), since the latter has a lower copper content (7 at.%) than the Cu-ZrN sample (11 at.%). Nevertheless, after activation both samples displayed a decrease in ion release. This behaviour may be explained based on the XPS results. The presence of CuO in the Cu-ZrON-DC100 (A) may explain the lower Cu^{2+} ions release in the NaCl solution, which was the electrolyte used in the ICP analysis. In this sense, the antibacterial activity in these types of coatings can mainly be caused by the CuO species. In fact, pure copper and copper oxide films were tested under the same conditions used for the Cu-Zr(O)N films, in order to verify antibacterial activity. Results showed a stronger antibacterial effect (higher inhibition halo) against *S. epidermidis* with the increase of oxygen content in the coating (see figure S2).

4. Conclusion

Zr(O)N and Cu-Zr(O)N coatings were obtained with different oxygen flows within duty cycle programmable pulse control by reactive magnetron sputtering with a wide range of colours, from golden to black tones. In relation to the chemical composition and crystal structure, Cu presence in Zr(O)N matrix was amorphous. After chemical activation, Cu rearranged into crystal oxides species. XPS analysis reported the presence of Cu, Cu_2O and $Cu(OH)_2$ in Cu-Zr(O)N, but in the Cu-ZrON-DC100 (A) sample, only CuO was detected. In fact, this is critical for antibacterial behaviour, since the Cu-ZrON-DC100 (A) was the only sample that possessed this feature. According to the ICP-OES results, Cu^{2+} ions release did not have influence on the antibacterial activity of the Cu-ZrON-DC100 (A). The formation of the CuO phase was crucial and it was only obtained after activation. The developed films could be a solution to combine aesthetical and antibacterial properties with a sustainable and low-cost element such as copper.

Acknowledgements

This research is sponsored by FEDER funds through the COMPETE program - Competitive Factors Operational Program - and by national funds through FCT - Foundation for Science and Technology - under the scope of the strategic funding of co-financed *via* UIDB/00285/2020 and UIDB/04650/2020 unit and BioTecNorte operation (NORTE-01-0145-FEDER-000004) funded by the European Regional Development Fund under the scope of Norte2020 - Programa Operacional Regional do Norte, On-SURF (co-financed via FEDER (PT2020) POCI-01-0247-FEDER-546024521; The authors also thank the financial support in the framework of HEALTHYDENT - POCI-01-0145-FEDER-030708) and ATRITO-0 (co-financed via FEDER (PT2020) POCI-01-0145-FEDER-030446.

Bibliography

[1] D.M. Yebra, S. Kiil, K. Dam-Johansen, Antifouling technology - Past, present and future steps towards efficient and environmentally friendly antifouling coatings, Prog. Org. Coatings. 50 (2004) 75–104. https://doi.org/10.1016/j.porgcoat.2003.06.001.

[2] Y.Y. Chang, H.L. Huang, Y.C. Chen, J.C. Weng, C.H. Lai, Characterization and antibacterial performance of ZrNO-Ag coatings, Surf. Coatings Technol. 231 (2013) 224–228. https://doi.org/10.1016/j.surfcoat.2012.05.084.

[3] J. Osés, G. Fuentes, J. Palacio, J. Esparza, J. García, R. Rodríguez, Antibacterial Functionalization of PVD Coatings on Ceramics, Coatings. 8 (2018) 197. https://doi.org/10.3390/coatings8050197.

[4] Y. Wu, X. Wu, G. Li, G. Li, Microstructure and mechanical properties of reactively sputtered Ti(O,N) coatings, Int. J. Refract. Met. Hard Mater. 26 (2008) 461–464. https://doi.org/10.1016/j.ijrmhm.2007.11.005.

[5] S. Lin, J. Zhang, R. Zhu, S. Fu, D. Yun, Effects of sputtering pressure on microstructure and mechanical properties of ZrN films deposited by magnetron sputtering, Mater. Res. Bull. 105 (2018) 231–236. https://doi.org/10.1016/j.materresbull.2018.04.054.

[6] P. Gu, X. Zhu, J. Li, H. Wu, D. Yang, Influence of substrate and Ar/N2 gas flow ratio on structural, optical and electrical properties of TiN thin films synthetized by DC magnetron sputtering, J. Mater. Sci. Mater. Electron. 29 (2018) 9893–9900. https://doi.org/10.1007/s10854-018-9031-2.

[7] S.K. Rawal, A.K. Chawla, R. Jayaganthan, R. Chandra, The influence of various sputtering parameters on structural, wettability and optical properties of Zr2ON2 thin films, Mater. Sci. Eng. B Solid-State Mater. Adv. Technol. 181 (2014) 16–23. https://doi.org/10.1016/j.mseb.2013.11.003.

[8] B. Subramanian, C. V. Muraleedharan, R. Ananthakumar, M. Jayachandran, A comparative study of titanium nitride (TiN), titanium oxy nitride (TiON) and titanium aluminum nitride (TiAlN), as surface coatings for bio implants, Surf. Coatings Technol. 205 (2011) 5014–5020. https://doi.org/10.1016/j.surfcoat.2011.05.004.

[9] C. Rebholz, H. Ziegele, A. Leyland, A. Matthews, Structure, mechanical and tribological properties of nitrogen-containing chromium coatings prepared by reactive magnetron sputtering, Surf. Coatings Technol. 115 (1999) 222–229. https://doi.org/10.1016/S0257-8972(99)00240-6.

[10] P. Carvalho, F. Vaz, L. Rebouta, L. Cunha, C.J. Tavares, C. Moura, E. Alves, A. Cavaleiro,

P. Goudeau, E. Le Bourhis, J.P. Rivìre, J.F. Pierson, O. Banakh, Structural, electrical, optical, and mechanical characterizations of decorative ZrOxNy thin films, J. Appl. Phys. 98 (2005). https://doi.org/10.1063/1.1990261.

[11] M.A. Signore, A. Rizzo, L. Mirenghi, M.A. Tagliente, A. Cappello, Characterization of zirconium oxynitride films obtained by radio frequency magnetron reactive sputtering, Thin Solid Films. 515 (2007) 6798–6804. https://doi.org/10.1016/j.tsf.2007.02.033.

[12] H. Iwata, H. Ishii, D. Kato, S. Kawashima, K. Kodama, M. Furusawa, M. Tanaka, T. Sekiya, Deposition of ZrON thin films by reactive magnetron sputtering using a hollow cylindrical target, J. Vac. Sci. Technol. A. 36 (2018) 061509. https://doi.org/10.1116/1.5042439.

[13] H.S. Vanegas P, S. Calderon V, J.E. Alfonso O, J.J. Olaya F, P.J. Ferreira, S. Carvalho, Influence of silicon on the microstructure and the chemical properties of nanostructured ZrN-Si coatings deposited by means of pulsed-DC reactive magnetron sputtering, Appl. Surf. Sci. 481 (2019) 1249–1259. https://doi.org/10.1016/j.apsusc.2019.03.128.

[14] J.M. Chappé, A.C. Fernandes, L. Cunha, C. Moura, F. Vaz, N. Martin, D. Munteanu, B. Borcea, TiN-based decorative coatings: Colour change by addition of C and O, J. Optoelectron. Adv. Mater. 10 (2008) 900–903.

[15] J.D. Castro, E. Carneiro, S.M. Marques, B. Figueiredo, A.J. Pontes, Á.M. Sampaio, I. Carvalho, M. Henriques, P.J.S. Cruz, S. Carvalho, Surface functionalization of 3D printed structures: Aesthetic and antibiofouling properties, Surf. Coatings Technol. (2020) 125464. https://doi.org/10.1016/j.surfcoat.2020.125464.

[16] F. Vaz, P. Carvalho, L. Cunha, L. Rebouta, C. Moura, E. Alves, A.R. Ramos, A. Cavaleiro, P. Goudeau, J.P. Rivière, Property change in ZrNxOy thin films: Effect of the oxygen fraction and bias voltage, Thin Solid Films. 469–470 (2004) 11–17. https://doi.org/10.1016/j.tsf.2004.06.191.

[17] S. Rtimi, J. Kiwi, Recent advances on sputtered films with Cu in ppm concentrations leading to an acceleration of the bacterial inactivation, Catal. Today. 340 (2020) 347–362. https://doi.org/10.1016/j.cattod.2018.06.016.

[18] P.J. Kelly, H. Li, P.S. Benson, K.A. Whitehead, J. Verran, R.D. Arnell, I. Iordanova, Comparison of the tribological and antimicrobial properties of CrN/Ag, ZrN/Ag, TiN/Ag, and TiN/Cu nanocomposite coatings, Surf. Coatings Technol. 205 (2010) 1606–1610. https://doi.org/10.1016/j.surfcoat.2010.07.029.

[19] O. Baghriche, S. Rtimi, C. Pulgarin, R. Sanjines, J. Kiwi, Innovative TiO2 /Cu Nanosurfaces Inactivating Bacteria in the Minute Range under Low-Intensity Actinic Light, ACS Appl.

Mater. Interfaces. 4 (2012) 5234–5240. https://doi.org/10.1021/am301153j.

[20] European Chemical Society, Element Scarcity - EuChemS Periodic Table, (n.d.). https://www.euchems.eu/euchems-periodic-table/ (accessed December 11, 2020).

[21] N. Ghasemi, F. Jamali-Sheini, R. Zekavati, CuO and Ag/CuO nanoparticles: Biosynthesis and antibacterial properties, Mater. Lett. 196 (2017) 78–82. https://doi.org/10.1016/j.matlet.2017.02.111.

[22] X. He, G. Zhang, X. Wang, R. Hang, X. Huang, L. Qin, B. Tang, X. Zhang, Biocompatibility, corrosion resistance and antibacterial activity of TiO2/CuO coating on titanium, Ceram. Int. 43 (2017) 16185–16195. https://doi.org/10.1016/j.ceramint.2017.08.196.

[23] J.M. Chappé, N. Martin, J. Lintymer, F. Sthal, G. Terwagne, J. Takadoum, Titanium oxynitride thin films sputter deposited by the reactive gas pulsing process, Appl. Surf. Sci. 253 (2007) 5312–5316. https://doi.org/10.1016/j.apsusc.2006.12.004.

[24] N. Martin, J. Lintymer, J. Gavoille, J.M. Chappé, F. Sthal, J. Takadoum, F. Vaz, L. Rebouta, Reactive sputtering of TiOxNycoatings by the reactive gas pulsing process. Part I: Pattern and period of pulses, Surf. Coatings Technol. 201 (2007) 7720–7726. https://doi.org/10.1016/j.surfcoat.2007.03.002.

[25] N. Martin, J. Lintymer, J. Gavoille, J.M. Chappé, F. Sthal, J. Takadoum, F. Vaz, L. Rebouta, Reactive sputtering of TiOxNy coatings by the reactive gas pulsing process: Part III: The particular case of exponential pulses, Surf. Coatings Technol. 201 (2007) 7733–7738. https://doi.org/10.1016/j.surfcoat.2007.03.022.

[26] N. Martin, J. Lintymer, J. Gavoille, J.M. Chappé, F. Sthal, J. Takadoum, F. Vaz, L. Rebouta, Reactive sputtering of TiOxNycoatings by the reactive gas pulsing process. Part II: The role of the duty cycle, Surf. Coatings Technol. 201 (2007) 7727–7732. https://doi.org/10.1016/j.surfcoat.2007.03.021.

[27] F. Vaz, P. Cerqueira, L. Rebouta, S.M.C. Nascimento, E. Alves, P. Goudeau, J.P. Rivière, K. Pischow, J. De Rijk, Structural, optical and mechanical properties of coloured TiNxOythin films, Thin Solid Films. 447–448 (2004) 449–454. https://doi.org/10.1016/S0040-6090(03)01123-4.

[28] I. Ferreri, S. Calderon V., R. Escobar Galindo, C. Palacio, M. Henriques, A.P. Piedade, S. Carvalho, Silver activation on thin films of Ag-ZrCN coatings for antimicrobial activity, Mater. Sci. Eng. C. 55 (2015) 547–555. https://doi.org/10.1016/j.msec.2015.05.071.

[29] A. International, Volume 3: Alloy Phase Diagrams, First, ASM International, 1992.

[30] A. Bauer, W. Kirby, J. Sherris, M. Turk, Antibiotic susceptibility testing by standard single

disk method, Am. J. Clin. Pathol. 45 (1966) 493–496.

[31] N.K. Manninen, S. V. Calderon, I. Carvalho, M. Henriques, A. Cavaleiro, S. Carvalho, Antibacterial Ag/a-C nanocomposite coatings: The influence of nano-galvanic a-C and Ag couples on Ag ionization rates, Appl. Surf. Sci. 377 (2016) 283–291. https://doi.org/10.1016/j.apsusc.2016.03.113.

[32] M. Ohring, Materials Science of Thin Films, Second Edition, 2002. https://doi.org/10.1016/B978-0-12-524975-1.50018-5.

[33] C. Moura, P. Carvalho, F. Vaz, L. Cunha, E. Alves, Raman spectra and structural analysis in ZrOxNy thin films, Thin Solid Films. 515 (2006) 1132–1137. https://doi.org/10.1016/j.tsf.2006.07.039.

[34] P. Carvalho, A.C. Fernandes, L. Rebouta, F. Vaz, L. Cunha, U. Kreissig, N.P. Barradas, A.R. Ramos, E. Alves, Compositional and structural changes in ZrOxNy films depending on growth condition, Nucl. Instruments Methods Phys. Res. Sect. B Beam Interact. with Mater. Atoms. 249 (2006) 458–461. https://doi.org/10.1016/j.nimb.2006.03.031.

[35] D.R. Lide, G. Baysinger, CRC Handbook of Chemistry and Physics, 92nd ed., CRC Press, 2011. https://doi.org/10.1201/9781315380476-3.

[36] X. Ma, C. Li, K. Bai, P. Wu, W. Zhang, Thermodynamic assessment of the Zr-N system, J. Alloys Compd. 373 (2004) 194–201. https://doi.org/10.1016/j.jallcom.2003.10.051.

[37] X. Yao, X. Zhang, H. Wu, L. Tian, Y. Ma, B. Tang, Microstructure and antibacterial properties of Cu-doped TiO2 coating on titanium by micro-arc oxidation, Appl. Surf. Sci. 292 (2014) 944–947. https://doi.org/10.1016/j.apsusc.2013.12.083.

[38] P. Carvalho, J. Borges, M.S. Rodrigues, N.P. Barradas, E. Alves, J.P. Espinós, A.R. González-Elipe, L. Cunha, L. Marques, M.I. Vasilevskiy, F. Vaz, Optical properties of zirconium oxynitride films: The effect of composition, electronic and crystalline structures, Appl. Surf. Sci. 358 (2015) 660–669. https://doi.org/10.1016/j.apsusc.2015.09.129.

[39] A. Alhussein, S. Achache, R. Deturche, F. Sanchette, C. Pulgarin, J. Kiwi, S. Rtimi, Beneficial effect of Cu on Ti-Nb-Ta-Zr sputtered uniform/adhesive gum films accelerating bacterial inactivation under indoor visible light, Colloids Surfaces B Biointerfaces. 152 (2017) 152–158. https://doi.org/10.1016/j.colsurfb.2017.01.020.

[40] R. Guan, H. Hashimoto, K.H. Kuo, Electron-microscopic study of the structure of metastable oxides formed in the initial stage of copper oxidation. II. Cu 8 O, Acta Crystallogr. Sect. B Struct. Sci. 40 (1984) 560–566. https://doi.org/10.1107/S010876818400269X.

[41] I. Milošev, H.-H. Strehblow, M. Gaberšček, B. Navinšek, Electrochemical Oxidation of ZrN Hard (PVD) Coatings Studied by XPS, Surf. Interface Anal. 24 (1996) 448–458. https://doi.org/10.1002/(SICI)1096-9918(199607)24:7<448::AID-SIA137>3.0.CO;2-F.

[42] P. Carvalho, J.M. Chappé, L. Cunha, S. Lanceros-Méndez, P. Alpuim, F. Vaz, E. Alves, C. Rousselot, J.P. Espinós, A.R. González-Elipe, Influence of the chemical and electronic structure on the electrical behavior of zirconium oxynitride films, J. Appl. Phys. 103 (2008) 104907. https://doi.org/10.1063/1.2927494.

[43] H. Wiame, M.A. Centeno, S. Picard, P. Bastians, P. Grange, Thermal oxidation under oxygen of zirconium nitride studied by XPS, DRIFTS, TG-MS, J. Eur. Ceram. Soc. 18 (1998) 1293–1299. https://doi.org/10.1016/s0955-2219(98)00056-9.

[44] J.S. Colligon, H. Kheyrandish, L.N. Lesnevsky, A. Naumkin, A. Rogozin, I.I. Shkarban, L. Vasilyev, V.E. Yurasova, Composition and chemical state of titanium nitride films obtained by different methods, Surf. Coatings Technol. 70 (1994) 9–17. https://doi.org/10.1016/0257-8972(94)90068-X.

[45] J.P. Abriata, J. Garcés, R. Versaci, The O−Zr (Oxygen-Zirconium) system, Bull. Alloy Phase Diagrams. 7 (1986) 116–124. https://doi.org/10.1007/BF02881546.

[46] L. Gribaudo, D. Arias, J. Abriata, The N-Zr (Nitrogen-Zirconium) System, J. Phase Equilibria. 15 (1994) 441–449. https://doi.org/10.1007/BF02647575.

[47] T. Mishima, M. Matsuda, M. Miyake, Visible-light photocatalytic properties and electronic structure of Zr-based oxynitride, Zr2ON2, derived from nitridation of ZrO2, Appl. Catal. A Gen. 324 (2007) 77–82. https://doi.org/10.1016/j.apcata.2007.03.017.

[48] P. Prieto, L. Galán, J.M. Sanz, Electronic structure of insulating zirconium nitride, Phys. Rev. B. 47 (1993) 1613–1615. https://doi.org/10.1103/PhysRevB.47.1613.

[49] I. Platzman, R. Brener, H. Haick, R. Tannenbaum, Oxidation of polycrystalline copper thin films at ambient conditions, J. Phys. Chem. C. 112 (2008) 1101–1108. https://doi.org/10.1021/jp076981k.

[50] M.C. Biesinger, Advanced analysis of copper X-ray photoelectron spectra, Surf. Interface Anal. 49 (2017) 1325–1334. https://doi.org/10.1002/sia.6239.

[51] C. Morant, J.M. Sanz, L. Galán, L. Soriano, F. Rueda, An XPS study of the interaction of oxygen with zirconium, Surf. Sci. 218 (1989) 331–345. https://doi.org/10.1016/0039-6028(89)90156-8.

[52] Y. Alajlani, F. Placido, A. Barlow, H.O. Chu, S. Song, S. Ur Rahman, R. De Bold, D. Gibson, Characterisation of Cu2O, Cu4O3, and CuO mixed phase thin films produced by

microwave-activated reactive sputtering, Vacuum. 144 (2017) 217–228. https://doi.org/10.1016/j.vacuum.2017.08.005.

[53] N.S. McIntyre, S. Sunder, D.W. Shoesmith, F.W. Stanchell, Chemical Information From Xps - Applications To the Analysis of Electrode Surfaces., J. Vac. Sci. Technol. 18 (1980) 714–721. https://doi.org/10.1116/1.570934.

[54] J.P. Espinós, J. Morales, A. Barranco, A. Caballero, J.P. Holgado, A.R. González-Elipe, Interface Effects for Cu, CuO, and Cu2O Deposited on SiO2 and ZrO2. XPS Determination of the Valence State of Copper in Cu/SiO2 and Cu/ZrO2 Catalysts, J. Phys. Chem. B. 106 (2002) 6921–6929. https://doi.org/10.1021/jp014618m.

[55] Q. Huang, Y. Wang, J. Li, Preparation of solar selective absorbing CuO coating for medium temperature application, Front. Chem. Eng. China. 1 (2007) 256–260. https://doi.org/10.1007/s11705-007-0046-0.

[56] Y. Cudennec, A. Lecerf, The transformation of Cu(OH)2 into CuO, revisited, Solid State Sci. 5 (2003) 1471–1474. https://doi.org/10.1016/j.solidstatesciences.2003.09.009.

[57] C.I. da Silva Oliveira, D. Martinez-Martinez, L. Cunha, M.S. Rodrigues, J. Borges, C. Lopes, E. Alves, N.P. Barradas, M. Apreutesei, Zr-O-N coatings for decorative purposes: Study of the system stability by exploration of the deposition parameter space, Surf. Coatings Technol. 343 (2018) 30–37. https://doi.org/10.1016/j.surfcoat.2017.11.056.

[58] P. Carvalho, L. Cunha, E. Alves, N. Martin, E. Le Bourhis, F. Vaz, ZrOxNy decorative thin films prepared by the reactive gas pulsing process, J. Phys. D. Appl. Phys. 42 (2009). https://doi.org/10.1088/0022-3727/42/19/195501.

[59] P. Li, Z. Ding, Y. Yin, X. Yu, Y. Yuan, M. Brió Pérez, S. de Beer, G.J. Vancso, Y. Yu, S. Zhang, Cu2+-doping of polyanionic brushes: A facile route to prepare implant coatings with both antifouling and antibacterial properties, Eur. Polym. J. 134 (2020) 109845. https://doi.org/10.1016/j.eurpolymj.2020.109845.

[60] N. Matsumoto, K. Sato, K. Yoshida, K. Hashimoto, Y. Toda, Preparation and characterization of β-tricalcium phosphate co-doped with monovalent and divalent antibacterial metal ions, Acta Biomater. 5 (2009) 3157–3164. https://doi.org/10.1016/j.actbio.2009.04.010.

José D. Castro: Investigation, Formal analysis, Data curation, Writing – Original Draft & Visualization. **Maria J. Lima:** Investigation, Writing – Review & Editing. **Isabel Carvalho:** Investigation, Writing – Original Draft & Visualization. **Mariana Henriques:** Conceptualization, Methodology, Supervision, Writing – Review & Editing. **S. Carvalho:** Conceptualization, Methodology, Supervision, Writing – Review & Editing, Project administration & Funding acquisition.

Declaration of interests

☒ The authors declare that they have no known competing financial interests or personal relationships that could have appeared to influence the work reported in this paper.

☐The authors declare the following financial interests/personal relationships which may be considered as potential competing interests

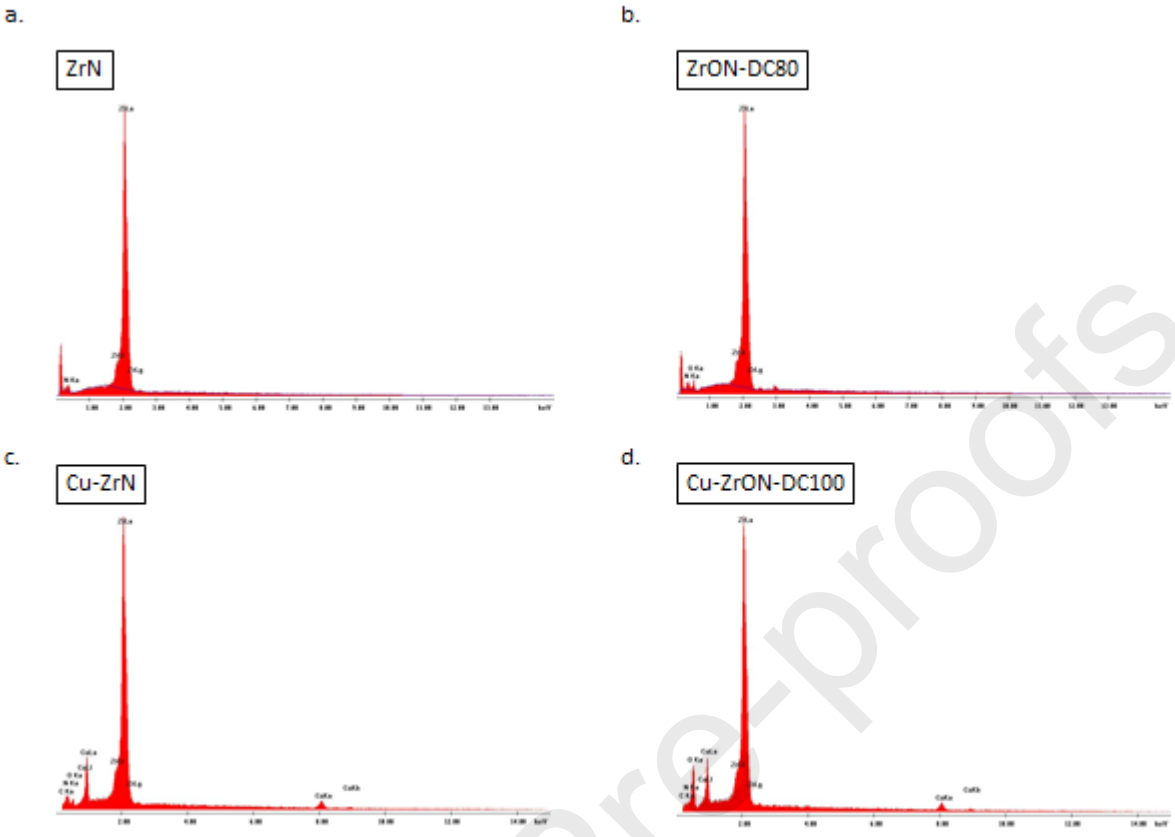

Figure 1. EDS patterns from (a) ZrN, (b) ZrON-DC80(b), (c) Cu-ZrN and (d) Cu-ZrON-DC100 coatings.

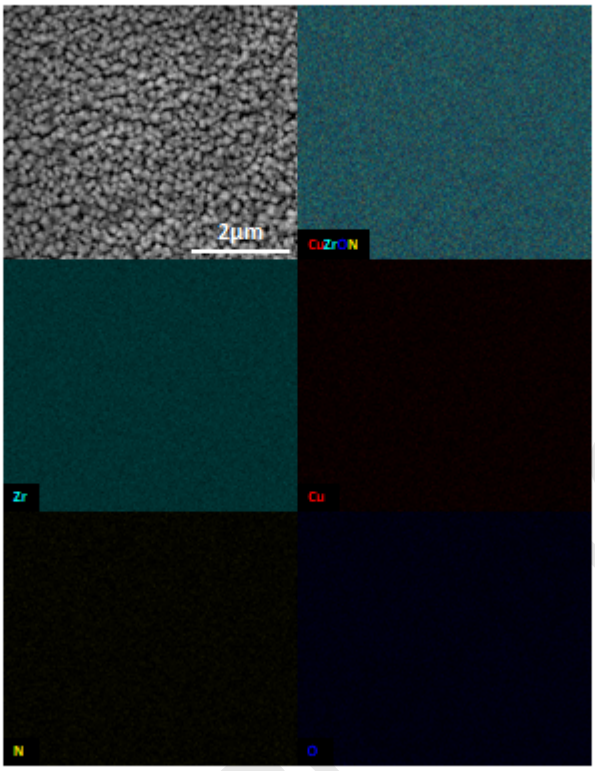

Figure 2. SEM-EDS Elemental mapping obtained from Cu-ZrON-DC100 sample.

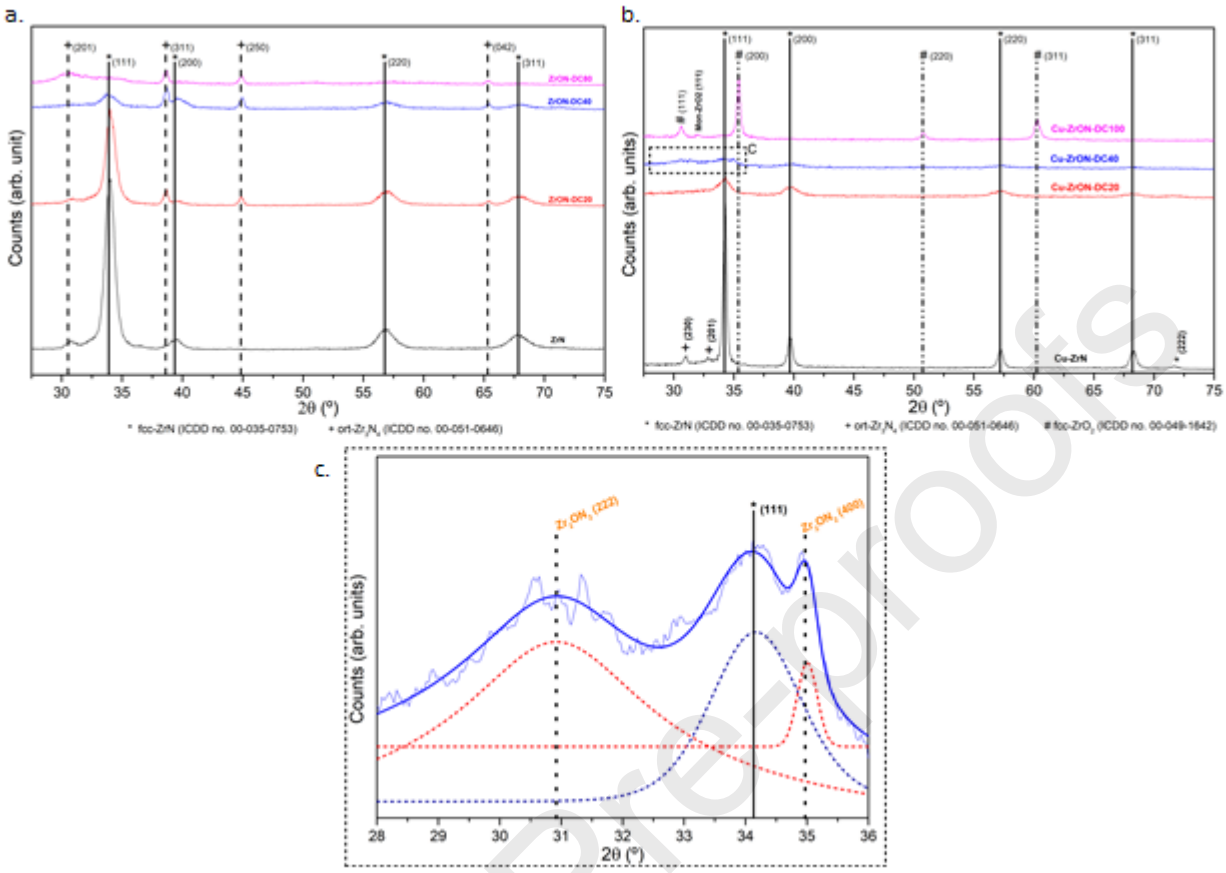

Figure 3. XRD patterns from undoped (a) and doped (b) films and deconvolution of peaks of Cu-ZrON-DC40 sample (a dotted rectangle in (b)) (c).

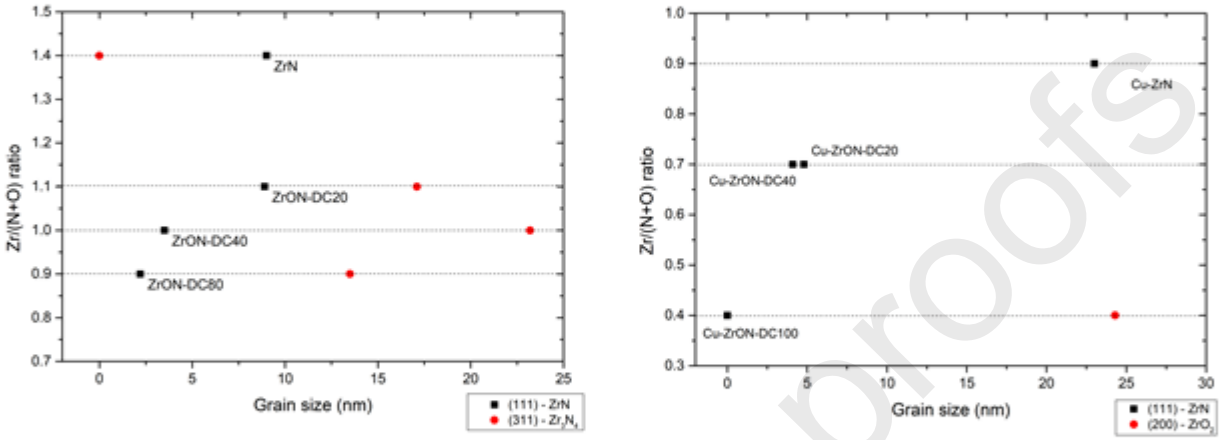

Figure 4. Grain size of Zr(O)N (left) and Cu-Zr(O)N (right) calculated from XRD diffractograms (figure 3) applying Scherrer formula.

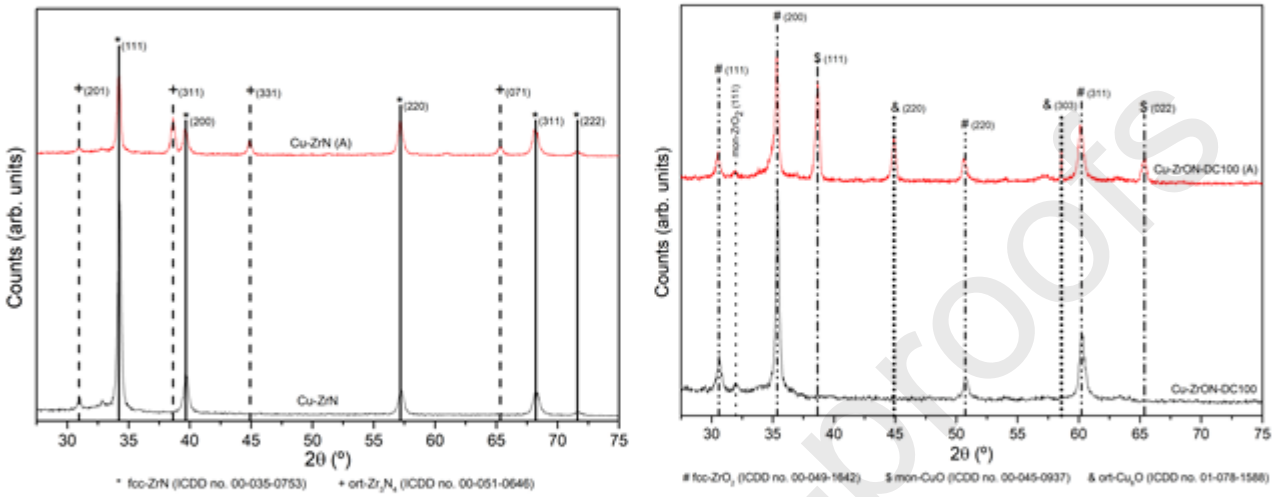

Figure 5. XRD diffractograms of Cu-ZrN (a) and Cu-ZrON-DC100 (b) coatings before and after activation (samples labelled with (A)).

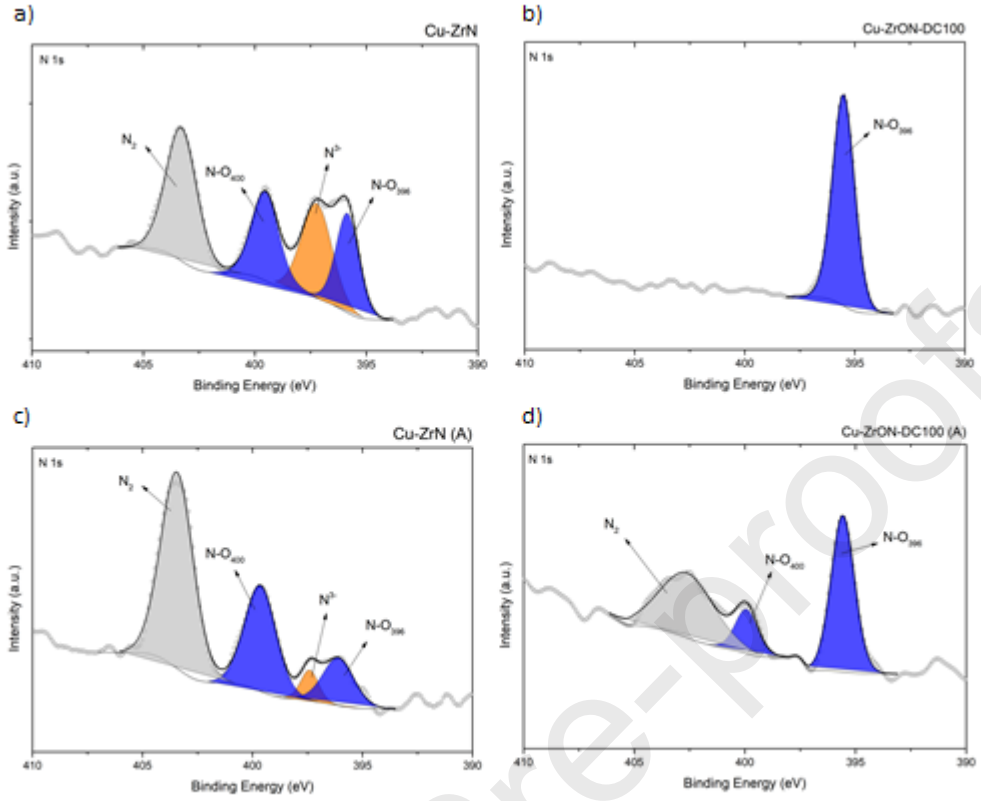

Figure 6. XPS spectra at N 1s level from studied samples before and after NaOCl treatment. (a) Cu-ZrN, (b) Cu-ZrON-DC100, (c) Cu-ZrN (A) and, (d) Cu-ZrON-DC100 (A).

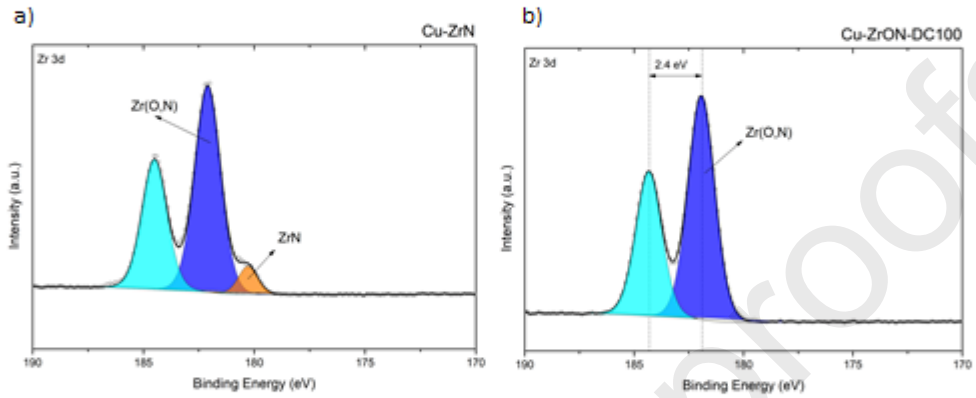

Figure 7. XPS spectra at Zr 3d level from studied samples. (a) Cu-ZrN, (b) Cu-ZrON-DC100.

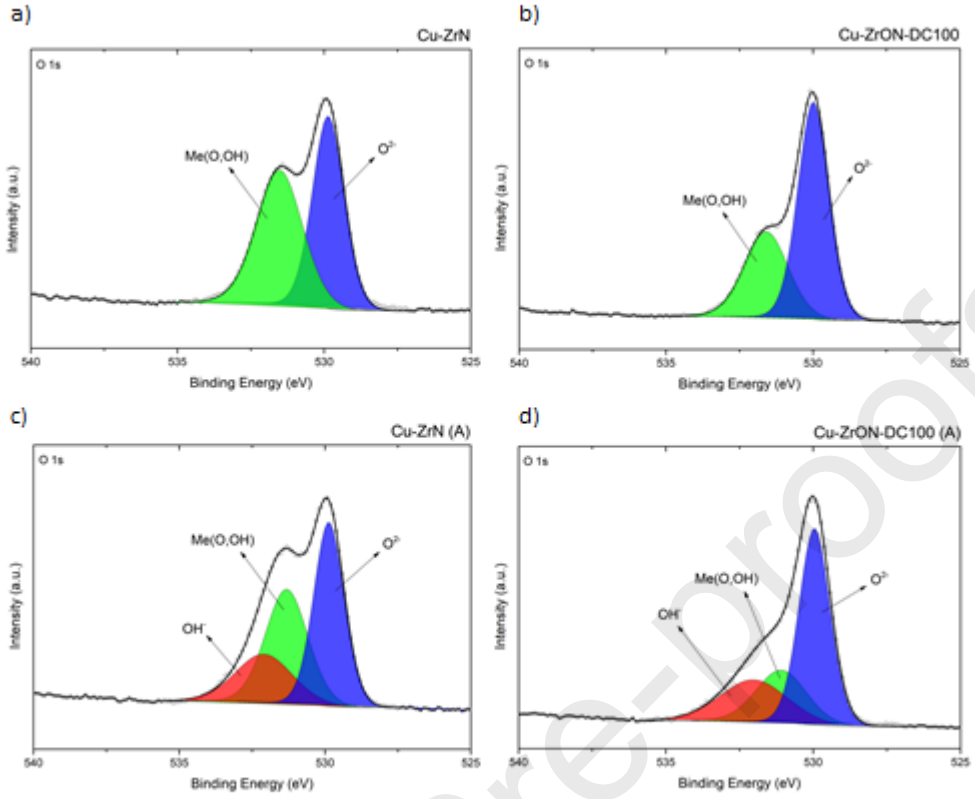

Figure 8. XPS spectra at O 1s level from studied samples before and after NaOCl treatment. (a) Cu-ZrN, (b) Cu-ZrON-DC100, (c) Cu-ZrN (A) and, (d) Cu-ZrON-DC100 (A).

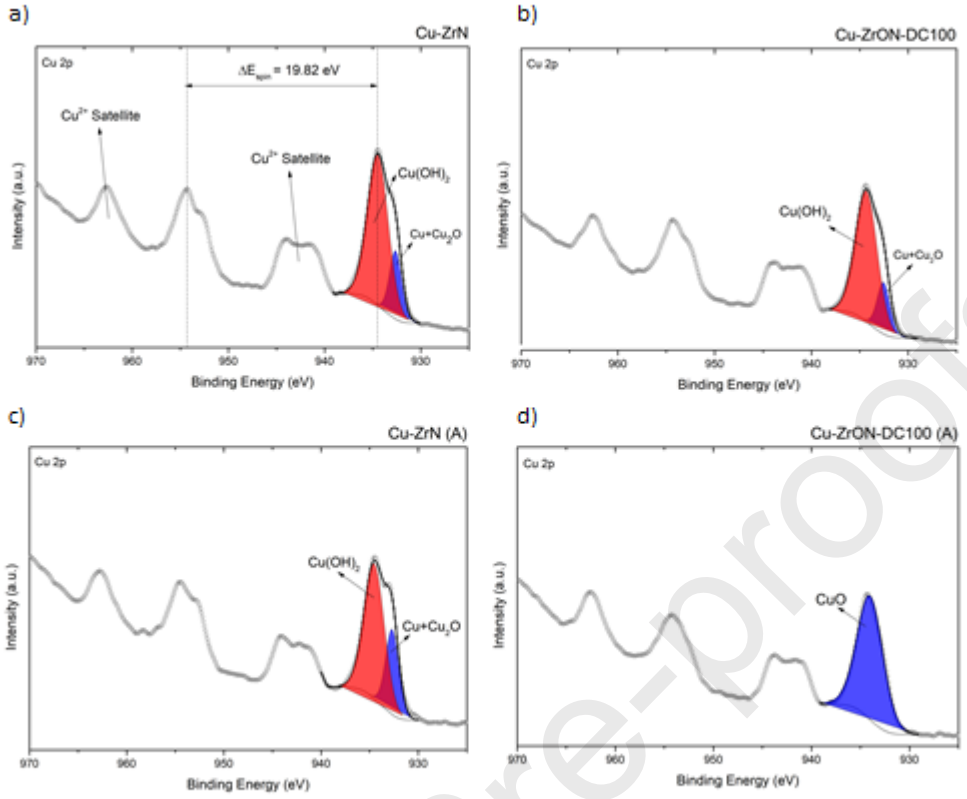

Figure 9. XPS spectra at Cu 2p level from studied samples before and after activation. (a) Cu-ZrN, (b) Cu-ZrON-DC100, (c) Cu-ZrN (A) and (d) Cu-ZrON-DC100 (A).

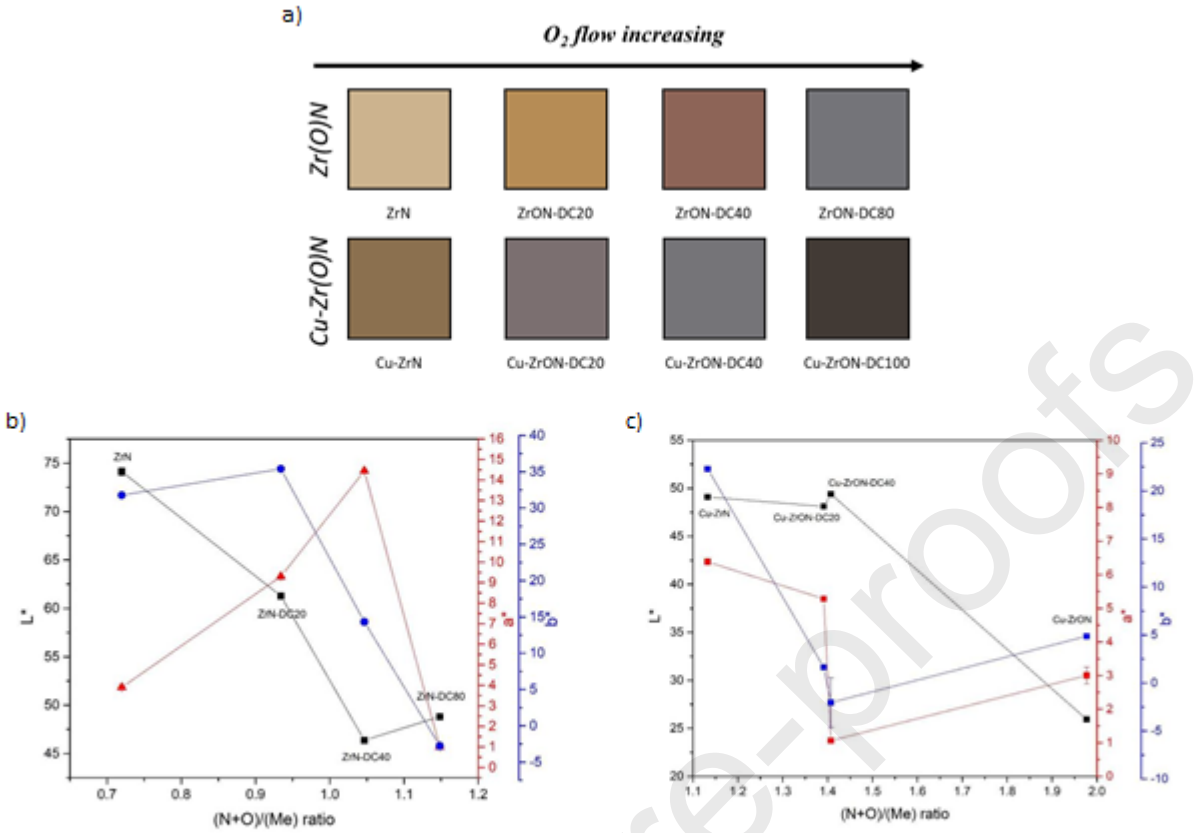

Figure 10. Obtained colours of all coatings according with non-metallic/metallic components ratio: a) colour chart, b) colorimetric parameters of undoped films and c) doped films.

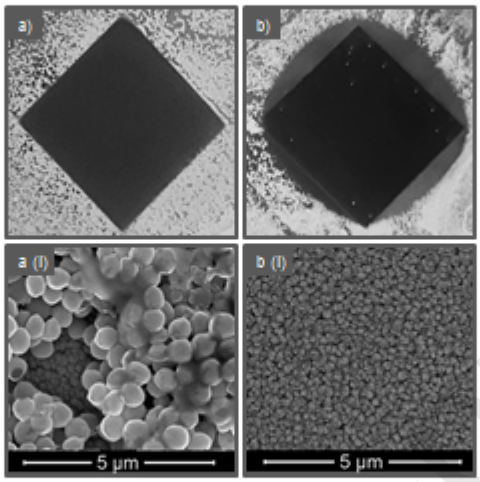

Figure 11. Halo test performed in Cu-ZrN (A) (a) and Cu-ZrON-DC100 (A) (b) coatings on SS316L substrates. a(i) and b(i) SEM images after halo test of Cu-ZrN (A) and Cu-ZrON-DC100 (A), respectively.

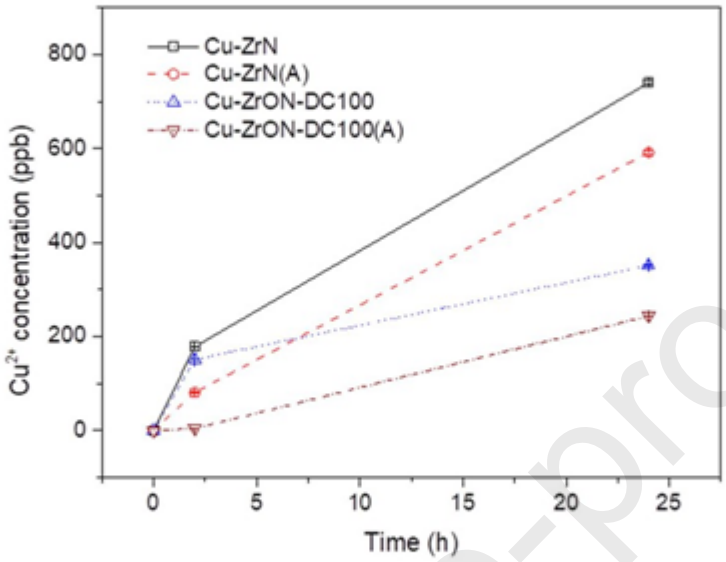

Figure 12. Cu^{2+} release along time determined by ICP−OES analysis.